

Amplitude Analysis of the Decay $B^0 \rightarrow K^+\pi^-\pi^0$

The *BABAR* Collaboration

March 24, 2019

Abstract

We report an updated amplitude analysis of the charmless hadronic decays of neutral B mesons to $K^+\pi^-\pi^0$. With a sample of 454 million $\Upsilon(4S) \rightarrow B\bar{B}$ decays collected by the *BABAR* detector at the PEP-II asymmetric-energy B Factory at SLAC, we measure the magnitudes and phases of the intermediate resonant and non-resonant amplitudes for B^0 and \bar{B}^0 decays and determine the corresponding CP -averaged fit fractions and charge asymmetries.

Submitted to the 33rd International Conference on High-Energy Physics, ICHEP 08,
30 July—5 August 2008, Philadelphia, Pennsylvania.

Stanford Linear Accelerator Center, Stanford University, Stanford, CA 94309

Work supported in part by Department of Energy contract DE-AC02-76SF00515.

The BABAR Collaboration,

B. Aubert, M. Bona, Y. Karyotakis, J. P. Lees, V. Poireau, E. Prencipe, X. Prudent, V. Tisserand
Laboratoire de Physique des Particules, IN2P3/CNRS et Université de Savoie, F-74941 Annecy-Le-Vieux, France

J. Garra Tico, E. Grauges
Universitat de Barcelona, Facultat de Física, Departament ECM, E-08028 Barcelona, Spain

L. Lopez^{ab}, A. Palano^{ab}, M. Pappagallo^{ab}
INFN Sezione di Bari^a; Dipartimento di Fisica, Università di Bari^b, I-70126 Bari, Italy

G. Eigen, B. Stugu, L. Sun
University of Bergen, Institute of Physics, N-5007 Bergen, Norway

G. S. Abrams, M. Battaglia, D. N. Brown, R. N. Cahn, R. G. Jacobsen, L. T. Kerth, Yu. G. Kolomensky, G. Lynch,
I. L. Osipenkov, M. T. Ronan,¹ K. Tackmann, T. Tanabe
Lawrence Berkeley National Laboratory and University of California, Berkeley, California 94720, USA

C. M. Hawkes, N. Soni, A. T. Watson
University of Birmingham, Birmingham, B15 2TT, United Kingdom

H. Koch, T. Schroeder
Ruhr Universität Bochum, Institut für Experimentalphysik 1, D-44780 Bochum, Germany

D. Walker
University of Bristol, Bristol BS8 1TL, United Kingdom

D. J. Asgeirsson, B. G. Fulsom, C. Hearty, T. S. Mattison, J. A. McKenna
University of British Columbia, Vancouver, British Columbia, Canada V6T 1Z1

M. Barrett, A. Khan
Brunel University, Uxbridge, Middlesex UB8 3PH, United Kingdom

V. E. Blinov, A. D. Bukin, A. R. Buzykaev, V. P. Druzhinin, V. B. Golubev, A. P. Onuchin, S. I. Serednyakov,
Yu. I. Skovpen, E. P. Solodov, K. Yu. Todyshev
Budker Institute of Nuclear Physics, Novosibirsk 630090, Russia

M. Bondioli, S. Curry, I. Eschrich, D. Kirkby, A. J. Lankford, P. Lund, M. Mandelkern, E. C. Martin, D. P. Stoker
University of California at Irvine, Irvine, California 92697, USA

S. Abachi, C. Buchanan
University of California at Los Angeles, Los Angeles, California 90024, USA

J. W. Gary, F. Liu, O. Long, B. C. Shen,¹ G. M. Vitug, Z. Yasin, L. Zhang
University of California at Riverside, Riverside, California 92521, USA

V. Sharma
University of California at San Diego, La Jolla, California 92093, USA

C. Campagnari, T. M. Hong, D. Kovalskyi, M. A. Mazur, J. D. Richman
University of California at Santa Barbara, Santa Barbara, California 93106, USA

¹ Deceased

T. W. Beck, A. M. Eisner, C. J. Flacco, C. A. Heusch, J. Kroseberg, W. S. Lockman, A. J. Martinez, T. Schalk,
B. A. Schumm, A. Seiden, M. G. Wilson, L. O. Winstrom

University of California at Santa Cruz, Institute for Particle Physics, Santa Cruz, California 95064, USA

C. H. Cheng, D. A. Doll, B. Echenard, F. Fang, D. G. Hitlin, I. Narsky, T. Piatenko, F. C. Porter
California Institute of Technology, Pasadena, California 91125, USA

R. Andreassen, G. Mancinelli, B. T. Meadows, K. Mishra, M. D. Sokoloff
University of Cincinnati, Cincinnati, Ohio 45221, USA

P. C. Bloom, W. T. Ford, A. Gaz, J. F. Hirschauer, M. Nagel, U. Nauenberg, J. G. Smith, K. A. Ulmer,
S. R. Wagner
University of Colorado, Boulder, Colorado 80309, USA

R. Ayad,² A. Soffer,³ W. H. Toki, R. J. Wilson
Colorado State University, Fort Collins, Colorado 80523, USA

D. D. Altenburg, E. Feltresi, A. Hauke, H. Jasper, M. Karbach, J. Merkel, A. Petzold, B. Spaan, K. Wacker
Technische Universität Dortmund, Fakultät Physik, D-44221 Dortmund, Germany

M. J. Kobel, W. F. Mader, R. Nogowski, K. R. Schubert, R. Schwierz, A. Volk
Technische Universität Dresden, Institut für Kern- und Teilchenphysik, D-01062 Dresden, Germany

D. Bernard, G. R. Bonneaud, E. Latour, M. Verderi
Laboratoire Leprince-Ringuet, CNRS/IN2P3, Ecole Polytechnique, F-91128 Palaiseau, France

P. J. Clark, S. Playfer, J. E. Watson
University of Edinburgh, Edinburgh EH9 3JZ, United Kingdom

M. Andreotti^{ab}, D. Bettoni^a, C. Bozzi^a, R. Calabrese^{ab}, A. Cecchi^{ab}, G. Cibinetto^{ab}, P. Franchini^{ab}, E. Luppi^{ab},
M. Negrini^{ab}, A. Petrella^{ab}, L. Piemontese^a, V. Santoro^{ab}
INFN Sezione di Ferrara^a; Dipartimento di Fisica, Università di Ferrara^b, I-44100 Ferrara, Italy

R. Baldini-Ferroli, A. Calcaterra, R. de Sangro, G. Finocchiaro, S. Pacetti, P. Patteri, I. M. Peruzzi,⁴ M. Piccolo,
M. Rama, A. Zallo
INFN Laboratori Nazionali di Frascati, I-00044 Frascati, Italy

A. Buzzo^a, R. Contri^{ab}, M. Lo Vetere^{ab}, M. M. Macri^a, M. R. Monge^{ab}, S. Passaggio^a, C. Patrignani^{ab},
E. Robutti^a, A. Santroni^{ab}, S. Tosi^{ab}
INFN Sezione di Genova^a; Dipartimento di Fisica, Università di Genova^b, I-16146 Genova, Italy

K. S. Chaisanguanthum, M. Morii
Harvard University, Cambridge, Massachusetts 02138, USA

A. Adametz, J. Marks, S. Schenk, U. Uwer
Universität Heidelberg, Physikalisches Institut, Philosophenweg 12, D-69120 Heidelberg, Germany

V. Klose, H. M. Lacker
Humboldt-Universität zu Berlin, Institut für Physik, Newtonstr. 15, D-12489 Berlin, Germany

² Now at Temple University, Philadelphia, Pennsylvania 19122, USA

³ Now at Tel Aviv University, Tel Aviv, 69978, Israel

⁴ Also with Università di Perugia, Dipartimento di Fisica, Perugia, Italy

D. J. Bard, P. D. Dauncey, J. A. Nash, M. Tibbetts
Imperial College London, London, SW7 2AZ, United Kingdom

P. K. Behera, X. Chai, M. J. Charles, U. Mallik
University of Iowa, Iowa City, Iowa 52242, USA

J. Cochran, H. B. Crawley, L. Dong, W. T. Meyer, S. Prell, E. I. Rosenberg, A. E. Rubin
Iowa State University, Ames, Iowa 50011-3160, USA

Y. Y. Gao, A. V. Gritsan, Z. J. Guo, C. K. Lae
Johns Hopkins University, Baltimore, Maryland 21218, USA

N. Arnaud, J. Béquilleux, A. D’Orazio, M. Davier, J. Firmino da Costa, G. Grosdidier, A. Höcker, V. Lepeltier, F. Le Diberder, A. M. Lutz, S. Pruvot, P. Roudeau, M. H. Schune, J. Serrano, V. Sordini,⁵ A. Stocchi, G. Wormser
Laboratoire de l’Accélérateur Linéaire, IN2P3/CNRS et Université Paris-Sud 11, Centre Scientifique d’Orsay, B. P. 34, F-91898 Orsay Cedex, France

D. J. Lange, D. M. Wright
Lawrence Livermore National Laboratory, Livermore, California 94550, USA

I. Bingham, J. P. Burke, C. A. Chavez, J. R. Fry, E. Gabathuler, R. Gamet, D. E. Hutchcroft, D. J. Payne, C. Touramanis
University of Liverpool, Liverpool L69 7ZE, United Kingdom

A. J. Bevan, C. K. Clarke, K. A. George, F. Di Lodovico, R. Sacco, M. Sigamani
Queen Mary, University of London, London, E1 4NS, United Kingdom

G. Cowan, H. U. Flaecher, D. A. Hopkins, S. Paramesvaran, F. Salvatore, A. C. Wren
University of London, Royal Holloway and Bedford New College, Egham, Surrey TW20 0EX, United Kingdom

D. N. Brown, C. L. Davis
University of Louisville, Louisville, Kentucky 40292, USA

A. G. Denig M. Fritsch, W. Gradl, G. Schott
Johannes Gutenberg-Universität Mainz, Institut für Kernphysik, D-55099 Mainz, Germany

K. E. Alwyn, D. Bailey, R. J. Barlow, Y. M. Chia, C. L. Edgar, G. Jackson, G. D. Lafferty, T. J. West, J. I. Yi
University of Manchester, Manchester M13 9PL, United Kingdom

J. Anderson, C. Chen, A. Jawahery, D. A. Roberts, G. Simi, J. M. Tuggle
University of Maryland, College Park, Maryland 20742, USA

C. Dallapiccola, X. Li, E. Salvati, S. Saremi
University of Massachusetts, Amherst, Massachusetts 01003, USA

R. Cowan, D. Dujmic, P. H. Fisher, G. Sciolla, M. Spitznagel, F. Taylor, R. K. Yamamoto, M. Zhao
Massachusetts Institute of Technology, Laboratory for Nuclear Science, Cambridge, Massachusetts 02139, USA

P. M. Patel, S. H. Robertson
McGill University, Montréal, Québec, Canada H3A 2T8

⁵ Also with Università di Roma La Sapienza, I-00185 Roma, Italy

A. Lazzaro^{ab}, V. Lombardo^a, F. Palombo^{ab}

INFN Sezione di Milano^a; Dipartimento di Fisica, Università di Milano^b, I-20133 Milano, Italy

J. M. Bauer, L. Cremaldi R. Godang,⁶ R. Kroeger, D. A. Sanders, D. J. Summers, H. W. Zhao
University of Mississippi, University, Mississippi 38677, USA

M. Simard, P. Taras, F. B. Viaud

Université de Montréal, Physique des Particules, Montréal, Québec, Canada H3C 3J7

H. Nicholson

Mount Holyoke College, South Hadley, Massachusetts 01075, USA

G. De Nardo^{ab}, L. Lista^a, D. Monorchio^{ab}, G. Onorato^{ab}, C. Sciacca^{ab}

INFN Sezione di Napoli^a; Dipartimento di Scienze Fisiche, Università di Napoli Federico II^b, I-80126 Napoli, Italy

G. Raven, H. L. Snoek

NIKHEF, National Institute for Nuclear Physics and High Energy Physics, NL-1009 DB Amsterdam, The Netherlands

C. P. Jessop, K. J. Knoepfel, J. M. LoSecco, W. F. Wang

University of Notre Dame, Notre Dame, Indiana 46556, USA

G. Benelli, L. A. Corwin, K. Honscheid, H. Kagan, R. Kass, J. P. Morris, A. M. Rahimi, J. J. Regensburger,
S. J. Sekula, Q. K. Wong

Ohio State University, Columbus, Ohio 43210, USA

N. L. Blount, J. Brau, R. Frey, O. Igonkina, J. A. Kolb, M. Lu, R. Rahmat, N. B. Sinev, D. Strom, J. Strube,
E. Torrence

University of Oregon, Eugene, Oregon 97403, USA

G. Castelli^{ab}, N. Gagliardi^{ab}, M. Margoni^{ab}, M. Morandin^a, M. Posocco^a, M. Rotondo^a, F. Simonetto^{ab},
R. Stroili^{ab}, C. Voci^{ab}

INFN Sezione di Padova^a; Dipartimento di Fisica, Università di Padova^b, I-35131 Padova, Italy

P. del Amo Sanchez, E. Ben-Haim, H. Briand, G. Calderini, J. Chauveau, P. David, L. Del Buono, O. Hamon,
Ph. Leruste, J. Ocariz, A. Perez, J. Prendki, S. Sitt

*Laboratoire de Physique Nucléaire et de Hautes Energies, IN2P3/CNRS, Université Pierre et Marie Curie-Paris6,
Université Denis Diderot-Paris7, F-75252 Paris, France*

L. Gladney

University of Pennsylvania, Philadelphia, Pennsylvania 19104, USA

M. Biasini^{ab}, R. Covarelli^{ab}, E. Manoni^{ab},

INFN Sezione di Perugia^a; Dipartimento di Fisica, Università di Perugia^b, I-06100 Perugia, Italy

C. Angelini^{ab}, G. Batignani^{ab}, S. Bettarini^{ab}, M. Carpinelli^{ab,7}, A. Cervelli^{ab}, F. Forti^{ab}, M. A. Giorgi^{ab},
A. Lusiani^{ac}, G. Marchiori^{ab}, M. Morganti^{ab}, N. Neri^{ab}, E. Paoloni^{ab}, G. Rizzo^{ab}, J. J. Walsh^a

*INFN Sezione di Pisa^a; Dipartimento di Fisica, Università di Pisa^b; Scuola Normale Superiore di Pisa^c, I-56127
Pisa, Italy*

⁶ Now at University of South Alabama, Mobile, Alabama 36688, USA

⁷ Also with Università di Sassari, Sassari, Italy

D. Lopes Pegna, C. Lu, J. Olsen, A. J. S. Smith, A. V. Telnov

Princeton University, Princeton, New Jersey 08544, USA

F. Anulli^a, E. Baracchini^{ab}, G. Cavoto^a, D. del Re^{ab}, E. Di Marco^{ab}, R. Faccini^{ab}, F. Ferrarotto^a, F. Ferroni^{ab},
M. Gaspero^{ab}, P. D. Jackson^a, L. Li Gioi^a, M. A. Mazzoni^a, S. Morganti^a, G. Piredda^a, F. Polci^{ab}, F. Renga^{ab},
C. Voena^a

INFN Sezione di Roma^a; Dipartimento di Fisica, Università di Roma La Sapienza^b, I-00185 Roma, Italy

M. Ebert, T. Hartmann, H. Schröder, R. Waldi

Universität Rostock, D-18051 Rostock, Germany

T. Adye, B. Franek, E. O. Olaiya, F. F. Wilson

Rutherford Appleton Laboratory, Chilton, Didcot, Oxon, OX11 0QX, United Kingdom

S. Emery, M. Escalier, L. Esteve, S. F. Ganzhur, G. Hamel de Monchenault, W. Kozanecki, G. Vasseur, Ch. Yèche,
M. Zito

CEA, Irfu, SPP, Centre de Saclay, F-91191 Gif-sur-Yvette, France

X. R. Chen, H. Liu, W. Park, M. V. Purohit, R. M. White, J. R. Wilson

University of South Carolina, Columbia, South Carolina 29208, USA

M. T. Allen, D. Aston, R. Bartoldus, P. Bechtel, J. F. Benitez, R. Cenci, J. P. Coleman, M. R. Convery,
J. C. Dingfelder, J. Dorfan, G. P. Dubois-Felsmann, W. Dunwoodie, R. C. Field, A. M. Gabareen, S. J. Gowdy,
M. T. Graham, P. Grenier, C. Hast, W. R. Innes, J. Kaminski, M. H. Kelsey, H. Kim, P. Kim, M. L. Kocian,
D. W. G. S. Leith, S. Li, B. Lindquist, S. Luitz, V. Luth, H. L. Lynch, D. B. MacFarlane, H. Marsiske, R. Messner,
D. R. Muller, H. Neal, S. Nelson, C. P. O'Grady, I. Ofte, A. Perazzo, M. Perl, B. N. Ratcliff, A. Roodman,
A. A. Salnikov, R. H. Schindler, J. Schwiening, A. Snyder, D. Su, M. K. Sullivan, K. Suzuki, S. K. Swain,
J. M. Thompson, J. Va'vra, A. P. Wagner, M. Weaver, C. A. West, W. J. Wisniewski, M. Wittgen, D. H. Wright,
H. W. Wulsin, A. K. Yarritu, K. Yi, C. C. Young, V. Ziegler

Stanford Linear Accelerator Center, Stanford, California 94309, USA

P. R. Burchat, A. J. Edwards, S. A. Majewski, T. S. Miyashita, B. A. Petersen, L. Wilden

Stanford University, Stanford, California 94305-4060, USA

S. Ahmed, M. S. Alam, J. A. Ernst, B. Pan, M. A. Saeed, S. B. Zain

State University of New York, Albany, New York 12222, USA

S. M. Spanier, B. J. Wogslund

University of Tennessee, Knoxville, Tennessee 37996, USA

R. Eckmann, J. L. Ritchie, A. M. Ruland, C. J. Schilling, R. F. Schwitters

University of Texas at Austin, Austin, Texas 78712, USA

B. W. Drummond, J. M. Izen, X. C. Lou

University of Texas at Dallas, Richardson, Texas 75083, USA

F. Bianchi^{ab}, D. Gamba^{ab}, M. Pelliccioni^{ab}

INFN Sezione di Torino^a; Dipartimento di Fisica Sperimentale, Università di Torino^b, I-10125 Torino, Italy

M. Bomben^{ab}, L. Bosisio^{ab}, C. Cartaro^{ab}, G. Della Ricca^{ab}, L. Lanceri^{ab}, L. Vitale^{ab}

INFN Sezione di Trieste^a; Dipartimento di Fisica, Università di Trieste^b, I-34127 Trieste, Italy

V. Azzolini, N. Lopez-March, F. Martinez-Vidal, D. A. Milanes, A. Oyanguren

IFIC, Universitat de Valencia-CSIC, E-46071 Valencia, Spain

J. Albert, Sw. Banerjee, B. Bhuyan, H. H. F. Choi, K. Hamano, R. Kowalewski, M. J. Lewczuk, I. M. Nugent,
J. M. Roney, R. J. Sobie

University of Victoria, Victoria, British Columbia, Canada V8W 3P6

T. J. Gershon, P. F. Harrison, J. Ilic, T. E. Latham, G. B. Mohanty

Department of Physics, University of Warwick, Coventry CV4 7AL, United Kingdom

H. R. Band, X. Chen, S. Dasu, K. T. Flood, Y. Pan, M. Pierini, R. Prepost, C. O. Vucosalo, S. L. Wu

University of Wisconsin, Madison, Wisconsin 53706, USA

I. INTRODUCTION

Amplitude analyses of three-body decays of B mesons with no charm particle in the final state are well suited to study the Cabibbo-Kobayashi-Maskawa (CKM) framework [1] for charged current weak interactions. In the analysis of a Dalitz plot the strong phases between interfering resonances are measured and can be used to constrain the weak phases related to the CKM parameters that, in the Standard Model, govern CP -violation. Following the path [2, 3, 4] of the 3-pion B meson decays which give constraints on the CKM angle $\alpha_{\text{CKM}} \equiv \arg(-V_{td}V_{tb}^*/V_{ud}V_{ub}^*)$, it has been shown in [5, 6] that B decays into a kaon and two pions are sensitive to the angle $\gamma_{\text{CKM}} \equiv \arg(-V_{ud}V_{ub}^*/V_{cd}V_{cb}^*)$.

In this paper we present an amplitude analysis of the flavor-specific $B^0 \rightarrow K^+\pi^-\pi^0$ decay [7]. This analysis, an update to an earlier analysis [8], compares the Dalitz plots of the B^0 and \bar{B}^0 decays where $K\pi$ and $\pi\pi$ resonances interfere. In addition to enhanced statistics, we utilize improved track reconstruction, tagging information from the opposite B , and the measured B flight-time to improve the quality of the measurements. Previous measurements of the three-body final state [9, 10] and subdecays [11, 12] to a vector and a pseudoscalar meson have been published. Other $B \rightarrow K\pi\pi$ decays have been studied in [13, 14, 15, 16]. A phenomenological study of three-body B meson decays without charm in the final state is presented in [17].

This paper is organized as follows. We first present in Section II the decay model based on an isobar expansion of the three-body decay amplitude. The complex coefficients of the expansion are the unknowns we seek to determine by means of an unbinned extended maximum likelihood fit. We describe the detector and dataset in Section III, the procedure used to select the data sample in Section IV, and the fit method in Section V. The results are then described in Section VI together with the accounting of the systematic uncertainties in Section VII. Finally in Section VIII, we summarize our findings.

II. DECAY AMPLITUDES

The $B^0 \rightarrow K^+\pi^-\pi^0$ decay amplitude is a function of two independent kinematic variables commonly chosen to be the invariant masses squared⁸, $x = m_{K^\pm\pi^\mp}^2$ and $y = m_{K^\pm\pi^0}^2$. The Dalitz plot (DP) is the x, y two-dimensional distribution. It is customary to express the decay amplitude as a sum over intermediate (isobar) states:

$$\mathcal{A}(x, y) = \sum_j a_j f_j(x, y), \quad (1)$$

and similarly for the $\bar{B}^0 \rightarrow K^-\pi^+\pi^0$ Dalitz plot,

$$\bar{\mathcal{A}}(x, y) = \sum_j \bar{a}_j f_j(x, y). \quad (2)$$

The complex isobar coefficients a_j are parameterized by:

$$a_j = c_j(1 + b_j)e^{i(\phi_j + \delta_j)} \quad (3)$$

$$\bar{a}_j = c_j(1 - b_j)e^{i(\phi_j - \delta_j)} \quad (4)$$

⁸ We use natural units where $\hbar = c = 1$ in our algebraic equations

and are constant over the Dalitz plot. The parameters b_k , ϕ_k , δ_k are related to the isobar fractions FF_k (CP -averaged over B^0 and \bar{B}^0), CP -violation charge asymmetries and phases by:

$$\begin{aligned}
FF_k &= \frac{\int_{DP} [|a_k f_k(x, y)|^2 + |\bar{a}_k \bar{f}_k(x, y)|^2] dx dy}{\int_{DP} [|\sum_j a_j f_j(x, y)|^2 + |\sum_j \bar{a}_j \bar{f}_j(x, y)|^2] dx dy} \\
A_{CP}^k &= \frac{|\bar{a}_k|^2 - |a_k|^2}{|\bar{a}_k|^2 + |a_k|^2} = \frac{-2b_k}{1 + b_k^2} \\
\Phi_k &= \phi_k + \delta_k, \\
\bar{\Phi}_k &= \phi_k - \delta_k
\end{aligned} \tag{5}$$

Note that, due to interference, the fractions FF_k in general do not add up to unity.

The decay dynamics of an intermediate state are specified by the $f_j(x, y)$ function which describes the Dalitz plot. For instance a resonance formed in the $K^+\pi^-$ system gives a contribution which factorizes as:

$$f_j(x, y) = R_j(x) \times T_j(x, y) \times W_j(x), \tag{6}$$

where $R_j(x)$ is the resonance mass distribution or lineshape and $T_j(x, y)$ models the angular dependence. The product of Blatt-Weisskopf damping factors, $W_j(x) = \sqrt{B_B(Rp^*(x)) B_j(Rq(x))}$ [18], slightly deviates from unity as a function of x through the breakup momenta⁹ of the (quasi) two body B and resonance decays multiplied by a range parameter R . The f_j are normalized,

$$\int_{DP} |f_j(x, y)|^2 dx dy = 1. \tag{7}$$

We use the Zemach tensor formalism [19, 20] for the angular distribution $T_j^{(J)}(x, y)$ of a process by which a pseudoscalar B meson produces a spin- J resonance in association with a bachelor pseudoscalar meson. For $J = 0, 1, 2$, we have:

$$\begin{aligned}
T_j^{(0)} &= 1, \\
T_j^{(1)} &= -2\vec{p} \cdot \vec{q}, \\
T_j^{(2)} &= \frac{4}{3}[3(\vec{p} \cdot \vec{q})^2 - (|\vec{p}||\vec{q}|)^2],
\end{aligned} \tag{8}$$

where¹⁰ $\vec{p}(x, y)$ ($\vec{q}(x)$) is the momentum vector of the bachelor particle (the resonance decay product Q defined below) measured in the resonance rest frame. For a neutral (charged) $K\pi$ resonance, Q is the pion (kaon), and for a dipion resonance, Q is the π^0 . Notice that these choices define for each two-body system the helicity angle $\theta_j = (\vec{p}_j, \vec{q}_j)$ between 0 and π .

Our nominal model (Table I) for the decay $B^0 \rightarrow K^+\pi^-\pi^0$ includes a nonresonant contribution which is uniformly distributed over the Dalitz plot, and seven resonant intermediate states: $\rho^-(770)K^+$, $\rho^-(1450)K^+$, $\rho^-(1700)K^+$, $K^*(892)^{+,0}\pi^-\pi^0$ and $(K\pi)_0^{*+,0}\pi^-\pi^0$. The notation for the last isobar component, introduced by the *BABAR* experiment [13], denotes phenomenological amplitudes describing the neutral and charged $K\pi$ S-waves each by a coherent superposition of an elastic effective range term and a term for the $K_0^*(1430)$ scalar resonance. It describes current knowledge on low energy $K\pi$ systems with a small number of parameters. In addition we include two non-interfering components for the decays $B^0 \rightarrow \bar{D}^0\pi^0 \rightarrow K^+\pi^-\pi^0$ and $B^0 \rightarrow D^-\pi^+\pi^0 \rightarrow K^+\pi^-\pi^0$. Variations in the nominal model are used to estimate the model-dependent systematic uncertainty in the results. The Gounaris-Sakurai (GS), relativistic Breit-Wigner (RBW), and LASS lineshapes are used to model the $R_j(x)$. Parameters are taken from [22] unless stated otherwise.

⁹ p^* , the momentum of the bachelor particle in the B meson rest frame, is equal to the breakup momentum of the studied B meson decay.

¹⁰ For simplicity, we have dropped the j index in \vec{p} and \vec{q} .

TABLE I: The *nominal model* for the decay $B^0 \rightarrow K^+ \pi^- \pi^0$ comprises a nonresonant part and seven intermediate states. The three types of lineshape are described in the text. The resonances masses and widths are from [22], except for the LASS shape [21]. We use the same LASS parameters for both neutral and charged $K\pi$ systems. *Additional resonances* that may contribute are included in extended models which we study to estimate the systematic uncertainties.

Intermediate state	Lineshape	Parameters
<i>Nominal model</i>		
Nonresonant	Constant	
$\rho^-(770)$	GS	$m = 768.5 \text{ MeV}/c^2$ $\Gamma^0 = 148.2 \text{ MeV}$
$\rho^-(1450)$	GS	$m = 1439 \text{ MeV}/c^2$ $\Gamma^0 = 550 \text{ MeV}$
$\rho^-(1700)$	GS	$m = 1795 \text{ MeV}/c^2$ $\Gamma^0 = 278 \text{ MeV}$
$K^{*+}(892)$	RBW	
$K^{*0}(892)$	RBW	
$(K\pi)_0^{*+}$ $(K\pi)_0^{*0}$	LASS	$m^0 = 1415 \pm 3 \text{ MeV}/c^2$ $\Gamma^0 = 300 \pm 6 \text{ MeV}$ cutoff $m_j^{max} = 1800 \text{ MeV}/c^2$ $a = 2.07 \pm 0.10 \text{ (GeV}/c)^{-1}$ $r = 3.32 \pm 0.34 \text{ (GeV}/c)^{-1}$
<i>Non-interfering Components</i>		
D^0	$mass = 1862.3$ $width = 7.1 \text{ MeV}/c^2$	Double Gaussian (From Data)
D^+	$mass = 1864.4$ $width = 9.9 \text{ MeV}/c^2$	Double Gaussian (From MC)
<i>Additional resonances</i>		
$K_2^*(1430)^{+,0}$	RBW	
$K^*(1680)^{+,0}$	RBW	

A. LINESHAPES

1. The relativistic Breit-Wigner distribution

The relativistic Breit-Wigner (RBW) parameterization is used for $K^*(892)^{+,0}$, $K_2^*(1430)^{+,0}$, and $K^*(1680)^{+,0}$:

$$R_j^{(J)}(x; m_j, \Gamma_j^0) = \frac{1}{m_j^2 - x - im_j \Gamma_j^{(J)}(x)}. \quad (9)$$

The mass-dependence of the total width $\Gamma_j^{(J)}$ can be ignored for high-mass states. For the low-mass states which decay only elastically, it is defined by

$$\Gamma_j^{(J)}(x) = \Gamma_j^0 \frac{m_j}{\sqrt{x}} \left(\frac{q(x)}{q(m_j^2)} \right)^{2J+1} \frac{B^{(J)}(Rq(x))}{B^{(J)}(Rq(m_j^2))}, \quad (10)$$

where m_j is the mass of the resonance j , $\Gamma_j^0 = \Gamma_j(m_j^2)$ its width, and the barrier factors (squares of the Blatt-Weisskopf damping factors [18]) are:

$$\begin{aligned} B^{(0)} &= 1, \\ B^{(1)} &= \frac{1}{1 + R^2 q^2}, \\ B^{(2)} &= \frac{1}{9 + 3R^2 q^2 + R^4 q^4}. \end{aligned} \tag{11}$$

All range parameters (R) are set to the values in the PDG [22].

2. The Gounaris-Sakurai distribution

The Gounaris-Sakurai (GS) parameterization [23] is used for $\rho^-(770)$, $\rho^-(1450)$ and $\rho^-(1700)$:

$$R_j^{GS}(x; m_j, \Gamma_j^0) = \frac{1 + d_j \Gamma_j^0 / m_j}{m_j^2 + g_j(x) - x - im_j \Gamma_j(x)}, \tag{12}$$

with the same x -dependence of the width as for the RBW. The expressions of the constant d_j and the function $g_j(x)$ in terms of m_j and Γ_j^0 are given in [23]. The parameters of the ρ lineshapes are taken from τ and $\pi\pi$ scattering in [24] and [25].

3. The LASS distribution

For the $K\pi S$ -wave amplitudes, $(K\pi)_0^{*+,0}$, which dominate for $m_{K\pi}$ below $m_j^{max} = 2 \text{ GeV}/c^2$, an effective-range parameterization was suggested [26] to describe the slowly increasing phase as a function of the $K\pi$ mass. We use the parameterization as in the LASS experiment [21], tuned for B decays:

$$\begin{aligned} R_j^{LASS}(x; m_j^0, \Gamma_j^0, a, r) &= \frac{\sqrt{x}}{q \cot \delta_B - iq} \\ &+ e^{2i\delta_B} \frac{m_j^0 \Gamma_j^0 \frac{m_j^0}{q_0}}{[(m_j^0)^2 - x] - im_j^0 \Gamma_j^0 \frac{q}{\sqrt{x}} \frac{m_j^0}{q_0}}, \end{aligned} \tag{13}$$

where

$$\cot \delta_B = \frac{1}{aq(x)} + \frac{1}{2} r q(x), \tag{14}$$

a is the scattering length, and r the effective range (Table I).

B. THE SQUARE DALITZ PLOT

The accessible phase space for charmless three-body B decays is unusually large. Most contributing resonances have masses much lower than the B mass. Hence signal events cluster along the Dalitz plot boundaries. This is also true for background events. Past experience has shown that another set of variables, defining the *Square Dalitz Plot* (SDP) is well suited to such configurations. It is defined by the mapping:

$$\begin{aligned} dx dy &\longrightarrow dm' d\theta' \\ m' &\equiv \frac{1}{\pi} \arccos\left(2 \frac{m - m_{\min}}{m_{\max} - m_{\min}} - 1\right), \quad \theta' \equiv \frac{1}{\pi} \theta, \end{aligned} \tag{15}$$

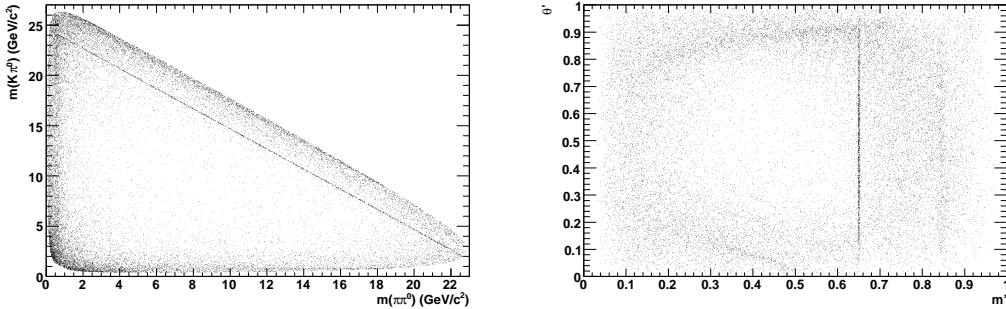


FIG. 1: The standard (a) and square (b) Dalitz plots of the selected data sample of 23683 events. The selection criteria are described in Sec. IV. The structures are more spread out in the square Dalitz plot. The $\bar{D}^0 \rightarrow K^+\pi^-$ narrow band is preserved with the choice made for the m' variable.

where $m = \sqrt{x}$ and θ are respectively the invariant mass and helicity angle of the $K^\pm\pi^\mp$ system. $m_{\max} = m_B - m_{\pi^0}$ and $m_{\min} = m_{K^+} + m_{\pi^-}$ are the kinematic limits of m . The new variables both range between 0 and 1. The standard and square Dalitz plots are shown for our data sample in Fig. 1.

III. THE BABAR DETECTOR AND DATASET

The data used in this analysis were collected with the *BABAR* detector at the PEP-II asymmetric energy e^+e^- storage rings between October 1999 and September 2007. This corresponds to an integrated luminosity of 413 fb^{-1} or approximately $N_{B\bar{B}} = 454 \pm 5$ million $B\bar{B}$ pairs taken on the peak of the $\Upsilon(4S)$ resonance (on resonance) and 41 fb^{-1} recorded at a center-of-mass (CM) energy 40 MeV below (off resonance).

A detailed description of the *BABAR* detector is given in [27]. Charged-particle trajectories are measured by a five-layer, double-sided silicon vertex tracker (SVT) and a 40-layer drift chamber (DCH) coaxial with a 1.5 T magnetic field. Charged-particle identification is achieved by combining the information from a ring-imaging Cherenkov device (DIRC) with the ionization energy loss (dE/dx) measurements from the DCH and SVT. Photons are detected in a CsI(Tl) electromagnetic calorimeter (EMC) inside the coil. Muon candidates are identified in the instrumented flux return of the solenoid. We use GEANT4-based [28] software to simulate the detector response and account for the varying beam and environmental conditions. Using this software, we generate signal and background Monte Carlo (MC) to estimate the efficiency and expected backgrounds in this analysis. Two samples of signal MC were used: one was generated with the Dalitz plot distribution observed in the previous analysis [8] while the other was generated with a phase-space distribution.

IV. EVENT SELECTION

A. SIGNAL SELECTION AND BACKGROUND REJECTION

To reconstruct $B^0 \rightarrow K^+\pi^-\pi^0$ decays, we select two charged particles and two photons. The charged particle candidates are required to have transverse momenta above 100 MeV/c and at least 12 hits in the DCH. They must not be identified as electrons or muons or protons. We select kaons and pions based on their signatures in the DIRC and DCH. The π^0 candidate is built from a pair of photon candidates, each with an energy greater than 50 MeV in the laboratory frame (LAB) and a lateral energy deposition profile in the EMC consistent with an electromagnetic shower. The invariant mass of a π^0 candidate must satisfy $|\frac{m_{\pi^0} - m_{\text{PDG}}}{\sigma_{m_{\pi^0}}}| < 3$. We also require $|\cos\theta_{\pi^0}^*|$, the modulus of the cosine of the angle the decay photons make with the π^0 momentum vector to be less than 0.95.

At the $\Upsilon(4S)$ resonance, B mesons are characterized by two nearly independent kinematic variables, the

beam energy substituted mass and the energy difference:

$$m_{\text{ES}} = \sqrt{(s/2 + \vec{p}_0 \cdot \vec{p}_B)^2/E_0^2 - p_B^2}, \quad (16)$$

$$\Delta E = E_B^* - \sqrt{s}/2, \quad (17)$$

where E and p are energy and momentum, the subscripts 0 and B refer to the e^+e^- -beam system and the B candidate respectively; s is the square of the center-of-mass energy and the asterisk labels the CM frame. We require that $5.272 < m_{\text{ES}} < 5.2875 \text{ GeV}/c^2$. To avoid a bias in the Dalitz plot from the dependence on the π^0 energy of the resolution in ΔE , we introduce the dimensionless quantity:

$$\Delta E' = \frac{\frac{\Delta E}{\sigma \Delta E} + m_0 + m_1 x + m_2 x^2 + m_3 x^3}{w_0 + w_1 x + w_2 x^2 + w_3 x^3} \quad (18)$$

where the coefficients are determined from fits to signal MC and $x = m_{K^\pm \pi^\mp}^2$. We require $|\Delta E'| \leq 2.1$.

Continuum $e^+e^- \rightarrow q\bar{q}$ ($q = u, d, s, c$) events are the dominant background. To enhance discrimination between signal and continuum, we select events by using a neural network [29] with an output NN which combines six discriminating variables: the angles of the B momentum and the B thrust axis with respect to the e^+ beam direction in the CM frame, the angle between the thrust axes of the signal B and other B , the zeroth and second order monomials L_0 and L_2 , and $\Delta z/\sigma(\Delta z)$, the flight distance between the two B s scaled by the error. The monomials are defined as $L_n \equiv \sum_i p_i \cdot |\cos \theta_i|^n$, where the sum runs over all charged and neutral particles in the event (except for those in the B candidate) whose momenta \vec{p}_i make angles θ_i with the B thrust axis. The neural network was trained on *off resonance* data and correctly reconstructed signal Monte Carlo events. We require $0.6 < NN$.

Approximately 15% of the signal events have multiple reconstructed B candidates (usually two). We select the candidate with the minimum value of:

$$\chi^2 = \left(\frac{m_{\pi^0} - m_{\text{PDG}}}{\sigma_{m_{\pi^0}}} \right)^2 + \chi_{\text{Vertex}}^2. \quad (19)$$

where χ_{Vertex}^2 is the χ^2 of the kinematic fit to the particles in the B meson candidate.

There are 23268 events in the data sample after the selection. The B meson candidate in each event is mass constrained to ensure that the measurement falls within the Dalitz plot boundary.

B. TRUTH-MATCHED AND SELF-CROSS-FEED SIGNAL EVENTS

Using the Monte Carlo simulation as in [3], we distinguish between the correctly reconstructed and the misreconstructed signal events. A correctly reconstructed event where the three particles of the B candidate match the generated ones, is called a *Truth-Matched* (TM) event. The TM PDFs describe correctly reconstructed events in the fit to data. A misreconstructed signal event contains a B meson which decays to the signal mode, but one or more reconstructed particles in the B candidate are not actually from the decay of that B . Misreconstructed signal is called *Self-Cross-Feed* (SCF). Misreconstruction is primarily due to the presence of low momentum pions. Consequently the efficiency $\varepsilon(m', \theta')$ to reconstruct an event either correctly or incorrectly varies across the Dalitz plot. The SCF fraction $f_{\text{SCF}}(m', \theta')$ is high, where the quality of the reconstruction is poor. This occurs in the corners of the Dalitz plot where one of the final-state particles has a low momentum in the LAB frame. These variations can be seen in Fig. 2 computed using high statistics Monte Carlo samples. It is important to keep a high efficiency in the Dalitz plot corners where the low-mass vector resonances interfere. Overall the total efficiency is close to 22.5% and the SCF fraction, averaged over the Dalitz plot, is $\sim 9\%$.

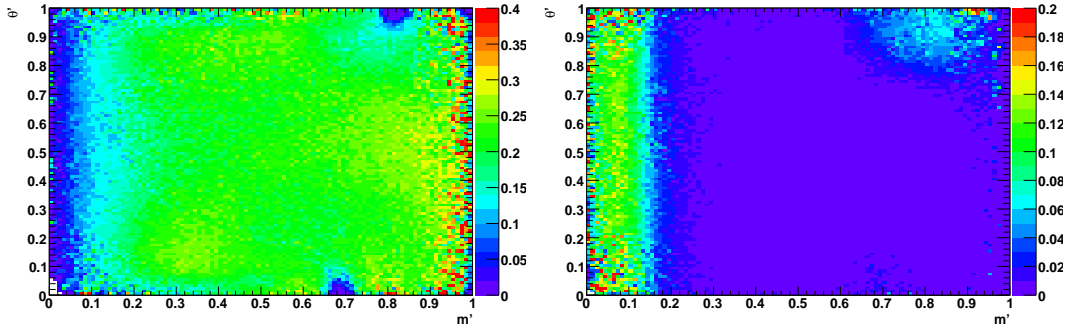


FIG. 2: Selection efficiency for truth-matched events on the left and SCF events on the right.

C. BACKGROUND

1. Continuum background

Although the neural network selection rejects 90% of the continuum events, this background is the dominant class of events in the data sample, representing about two thirds of its size.

2. Background from other B decays

Since there is no restriction on any two-body invariant mass of the final state particles, large backgrounds from other B decays occur. We use high statistics Monte Carlo samples to study these backgrounds. Conservative assumptions about unknown branching fractions are made. Inclusive and exclusive B decays with or without charm are grouped into nineteen classes to be used in the fit. Rates, and topological and kinematical similarities are studied to define the classes listed in Table II. Those backgrounds whose contributions are expected to be large (200 or more events) are varied in the fit while all others are fixed.

V. THE MAXIMUM LIKELIHOOD FIT

We perform an unbinned extended maximum likelihood fit to determine the total $B^0 \rightarrow K^+\pi^-\pi^0$ event yield, the magnitudes $c_j(1 \pm b_j)$ and phases $\phi_j \pm \delta_j$ of the complex isobar coefficients of the decay amplitude defined in Eq. 3. The fit uses the variables m' , θ' , m_{ES} , $\Delta E'$ and NN to discriminate signal from background. A simultaneous fit is performed using the B-tagging [30] category from the opposite B, for a further improvement in discriminating power. The variable label c denotes each of seven tagging categories defined in [30].

A. THE LIKELIHOOD FUNCTION

The selected on-resonance data sample consists of signal, continuum-background and background from other B decays. The probability density function (PDF) \mathcal{P}_i^c for an event i in tagging category c is the sum of the probability densities of all components, namely

TABLE II: The list of B -backgrounds retained for the fit (Section V). For each channel, we give (anticipating Section VI) either the fitted number of events in the data sample if its yield is allowed to vary in the fit procedure or the expected number otherwise.

Class	Mode	Events	
1	$B^0 \rightarrow K^{*0}(892)\gamma, K^{*0}(1430)\gamma$	187 ± 14	fixed
2	$\rho^+\pi^0$	11 ± 2	fixed
3	$f_0(980)K^+, K^{*+}\pi^0,$	48 ± 12	fixed
4	$K^{*+}K^-$	14 ± 10	fixed
5	$\pi^+\pi^-\pi^+$ Dalitz plot	8 ± 1	fixed
6	$K^+\pi^-\pi^+$ Dalitz plot	164 ± 9	fixed
7	$K^+\pi^0$	65 ± 3	fixed
8	$K^+\pi^-$	53 ± 2	fixed
9	$\pi^+\pi^-\pi^0$ Dalitz plot	109 ± 13	fixed
10	Generic $B \rightarrow$ charm with D^0	627 ± 60	varied
11	Generic $B \rightarrow$ charm with D^+	370 ± 80	varied
12	$K^{*+}a_1^-, K^{*0}\rho^0,$	9 ± 2	fixed
13	$K^+\eta\pi^-,$	8 ± 1	fixed
14	$\eta^1K^+,$	22 ± 1	fixed
15	$\rho^+\rho^-, a_1^+\pi^-$	27 ± 3	fixed
16	$K^{*0}\rho^+,$	15 ± 6	fixed
17	$K^{*+}\rho^-,$	21 ± 6	fixed
18	$\rho^+\rho^0, a_1^0\pi^+, a_1^+\pi^0$	50 ± 13	fixed
19	Combinatoric B Decays	660 ± 122	varied

$$\begin{aligned}
\mathcal{P}_i^c \equiv & N_{\text{sig}} f_{\text{sig}}^c \left[(1 - \bar{f}_{\text{SCF}}^c) \mathcal{P}_{\text{sig-TM},i}^c + \bar{f}_{\text{SCF}}^c \mathcal{P}_{\text{sig-SCF},i}^c \right] \\
& + N_{q\bar{q}}^c \frac{1}{2} (1 + q_{\text{tag},i} A_{q\bar{q},\text{tag}}) \mathcal{P}_{q\bar{q},i}^c \\
& + \sum_{j=1}^{N_{\text{class}}^{B,j}} N_{B,j} f_{B,j}^c \frac{1}{2} (1 + q_{\text{tag},i} A_{B,\text{tag},j}) \mathcal{P}_{B,ij}^c
\end{aligned} \tag{20}$$

where N_{sig} is the total number of $B^0 \rightarrow K^+\pi^-\pi^0$ signal events in the data sample; f_{sig}^c is the fraction of signal events that are tagged in category c ; \bar{f}_{SCF}^c is the fraction of SCF events in tagging category c , averaged over the DP; $\mathcal{P}_{\text{sig-TM},i}^c$ and $\mathcal{P}_{\text{sig-SCF},i}^c$ are the products of PDFs of the discriminating variables used in tagging category c for TM and SCF events, respectively; $N_{q\bar{q}}^c$ is the number of continuum events that are tagged in category c ; $q_{\text{tag},i}$ is the tag flavor of the event, and is equal to the charge of the kaon from the B decay; $A_{q\bar{q},\text{tag}}$ parameterizes possible tag asymmetry in continuum events; $\mathcal{P}_{q\bar{q},i}^c$ is the continuum PDF for tagging category c ; $N_{\text{class}}^{B,j}$ is the number of B -related background classes considered in the fit, namely nineteen; $N_{B,j}$ is the number of expected events in the B background class j ; $f_{B,j}^c$ is the fraction of B background events of class j that are tagged in category c ; $A_{B,\text{tag},j}$ describes a possible tag asymmetry in the B background class j ; $\mathcal{P}_{B,ij}^c$ is the B -background PDF for tagging category c and class j .

The PDFs \mathcal{P}_X^c ($X = \{\text{sig-TM}, \text{sig-SCF}, q\bar{q}, B\}$) are the product of the four PDFs of the discriminating

TABLE III: Summary of the PDF parameterizations. G=Gaussian, P1=1st order polynomial, NP=non-parametric. The notation (DP) designates a PDF with parameters which vary over the Dalitz plot. The Dalitz plot signal model is described in Section II.

Component	m_{ES}	$\Delta E'$	NN	Dalitz
signal (TM)	see text	G(DP)+P1(DP)	NP	see text
signal (SCF)	NP	NP	NP	see text
Continuum	Argus	P1	see text	NP
B backgrounds	NP	NP	NP	NP

variables ¹¹, $x_1 = m_{\text{ES}}$, $x_2 = \Delta E'$, $x_3 = \text{NN}$ output and the doublet $x_4 = \{m', \theta'\}$:

$$\mathcal{P}_{X,i(j)}^c \equiv \prod_{k=1}^4 P_{X,i(j)}^c(x_k), \quad (21)$$

where i is the event index and j is a B background class. The extended likelihood over all tagging categories is given by

$$\mathcal{L} \equiv \prod_{c=1}^7 e^{-\overline{N}^c} \prod_i^{\overline{N}^c} \mathcal{P}_i^c, \quad (22)$$

where \overline{N}^c is the total number of events expected in category c .

The correlations among the measurements are handled by building conditional PDFs where appropriate. The PDF parametrizations are given in Table III, and a summary of the parameters varied in the fit can be found in Section V.D.

B. THE DALITZ PROBABILITY DENSITY FUNCTIONS

Since the decay $B^0 \rightarrow K^+\pi^-\pi^0$ is flavor-specific (the charge of the kaon identifies the b flavor), the B^0 and \overline{B}^0 Dalitz plots are independent. However, because the backgrounds are essentially flavor blind, we get a more robust procedure by fitting them simultaneously. It is enough to describe only the B^0 Dalitz plot PDF. A change from \mathcal{A} to $\overline{\mathcal{A}}$ (Eq. (1) and (2)) accompanied by the interchange of the charges of the kaon and pion gives the \overline{B}^0 PDF.

1. Signal

The model for the distribution of signal events in the Dalitz plot has been described in Section II. The free parameters are c_j , b_j , ϕ_j , δ_j defined in Eq. (1) and (2) for all the intermediate states of the signal model given in Table I. Since the measurement is done relative to the $\rho^-(770)$ final state, the phases of this and the charge conjugate channels are fixed to zero. The amplitude of $B^0 \rightarrow \rho^-(770)K^+$ is also fixed but not that of $\overline{B}^0 \rightarrow \rho^+(770)K^-$ in order to be sensitive to direct CP -violation. The weak phase δ_j and CP violating amplitude b_j of the $\rho^-(1450)$ and $\rho^-(1700)$ are constrained to equal those of the $\rho^-(770)$ in the fit.

The normalization of the component signal PDFs:

$$\mathcal{P}_{TM,i} \propto \varepsilon_i(1 - f_{\text{SCF},i})|\det \mathcal{J}_i| |\mathcal{A}_i|^2, \quad (23)$$

¹¹ Not all the PDFs depend on the tagging category. The general notations $P_{X,i(j)}^c$ and $\mathcal{P}_{X,i(j)}^c$ are used for simplicity.

$$\mathcal{P}_{\text{SCF},i} \propto \varepsilon_i f_{\text{SCF},i} [|\det \mathcal{J}| |\mathcal{A}|^2 \otimes R_{\text{SCF}}]_i, \quad (24)$$

is model dependent. \mathcal{J} is the Jacobian matrix of the mapping to the square Dalitz plot. The symbol \otimes stands for a convolution and the R matrix is described below in Eq. (29). The normalization requires the computation of the integrals

$$\int_0^1 dm' \int_0^1 d\theta' \varepsilon (1 - f_{\text{SCF}}) |\det \mathcal{J}| f_k f_l^*, \quad (25)$$

$$\int_0^1 dm' \int_0^1 d\theta' \varepsilon f_{\text{SCF}} |\det \mathcal{J}| f_k f_l^*, \quad (26)$$

and

$$\int_0^1 dm' \int_0^1 d\theta' \varepsilon |\det \mathcal{J}| f_k f_l^*, \quad (27)$$

where the notations of Eq. (1) are used. The integrations over the square Dalitz plot are performed numerically. The weight

$$\bar{f}_{\text{SCF}} = \frac{\int_0^1 dm' \int_0^1 d\theta' \varepsilon f_{\text{SCF}} |\det \mathcal{J}| |\mathcal{A}|^2}{\int_0^1 dm' \int_0^1 d\theta' \varepsilon |\det \mathcal{J}| |\mathcal{A}|^2} \quad (28)$$

ensures that the total signal PDF is normalized. The PDF normalization depends on the decay dynamics and is computed iteratively. In practice the computation of \bar{f}_{SCF} rapidly converges to a value which we fix after a few exploratory fits.

Studies in simulation have shown that the experimental resolutions of m' and θ' need not be introduced in the TM signal PDF. However, misreconstructed events often incur large migrations, when the reconstructed m'_r, θ'_r are far from the true values m'_t, θ'_t . We use the Monte Carlo simulation to compute a normalized two-dimensional resolution function $R_{\text{SCF}}(m'_r, \theta'_r; m'_t, \theta'_t)$, with

$$\int_0^1 dm'_r \int_0^1 d\theta'_r R_{\text{SCF}}(m'_r, \theta'_r; m'_t, \theta'_t) = 1. \quad (29)$$

R_{SCF} is convolved with the signal model in the expression of \mathcal{P}_{SCF} in Eq. (24).

2. Background

Except for events coming from exclusive $B \rightarrow D$ decays, all background Dalitz PDF are modeled with non-parametric, smoothed, two-dimensional histograms. The continuum distributions are extracted from a combination of off resonance data and a sideband ($5.20 < m_{\text{ES}} < 5.25 \text{ GeV}/c^2$) of the on-resonance data from which the B -background has been subtracted. The square Dalitz plot is divided into eight regions where different smoothing parameters are applied in order to optimally reproduce the observed wide and narrow structures by using a two-dimensional kernel estimation technique [31]. For $0.64 < m' < 0.66$ and all θ' , a finely binned, unsmoothed histogram is used to follow the peak from the narrow D^0 continuum production. The B -background (Table II) Dalitz PDFs are obtained from the Monte Carlo simulation. For the components which model $b \rightarrow c$ decays with real D^0 mesons, a fine grained binning around the D mass is used to construct unsmoothed histograms.

C. THE OTHER PDFS

1. Signal

The m_{ES} distribution for signal events is parameterized as:

$$f(x = m_{\text{ES}}) = \exp \left[-\frac{(x - m)^2}{2\sigma_{\pm}^2 + \alpha_{\pm}(x - m)^2} \right] \quad (30)$$

where m and σ_{\pm} are floated in the data fit.

For SCF-signal events we use a non-parametric shape taken from the Monte Carlo simulation.

$\Delta E'$ is correlated with the Dalitz plot variables for TM-signal events. To account for the correlation, we choose the combination of a Gaussian and 1st order polynomial PDF. The mean and standard deviation of the Gaussian and slope of the polynomial vary linearly with $m_{K^{\pm}\pi^{\mp}}^2$. These parameters (intercept and slope) are free in the fit. A non-parametric shape taken from the Monte Carlo simulation is used for the SCF-signal $\Delta E'$ PDF.

The NN PDFs for TM and SCF events are non-parametric distributions taken from the Monte Carlo.

2. Background

We use the Argus function [32]

$$f(z = \frac{m_{\text{ES}}}{m_{\text{ES}}^{\text{max}}}) \propto z\sqrt{1-z^2}e^{-\xi(1-z^2)} \quad (31)$$

as the continuum m_{ES} PDF. The endpoint $m_{\text{ES}}^{\text{max}}$ is fixed to 5.2897 GeV/ c^2 and ξ is free in the fit. The $\Delta E'$ PDF is a linear polynomial whose slope is free to vary in the fit. The shape of the NN distribution for continuum is correlated with the event location in the Dalitz plot. To account for that effect we use for the NN PDF a function that varies with the closest distance Δ_{dalitz} between the point representing the event and the boundary of the standard Dalitz plot,

$$\begin{aligned} \mathcal{P}(NN; \Delta_{\text{dalitz}}) &= (1 - NN)^{k_1} \\ &\times (k_2 NN^2 + k_3 NN + k_4). \\ k_i &= q_i + p_i \cdot \Delta_{\text{dalitz}} \end{aligned} \quad (32)$$

The k_i are linear functions of Δ_{dalitz} where the q_i and p_i are varied in the likelihood fit.

We use non-parametric distributions taken from the Monte Carlo to describe m_{ES} , $\Delta E'$ and NN distributions for the B -background classes in Table II.

D. THE FIT PARAMETERS

The following parameters are varied in the fit:

- Yields for signal (N_{sig}), continuum ($N_{q\bar{q}}$) and three B background classes (c=10, 11 and 19 defined in Table II).
- CP -asymmetries for the continuum events.
- The global mean and slope(s), of the $\Delta E'$ distribution for the TM-signal (continuum) events.
- Parameters which describe the shape and correlation of the NN output and the event location in the Dalitz plot [Eq. (32)].
- The mean and widths of the function describing the m_{ES} distribution of the TM-signal events in addition to the ξ parameter of the Argus function describing the continuum m_{ES} shape.
- Thirty-two isobar magnitudes and phases. There are 10 intermediate states (7 resonances and a non-resonant term and two non-interfering D modes) and two Dalitz plots. We fix one reference magnitude, that of $B^0 \rightarrow \rho^-(770)K^+$ and two phases for the latter and its conjugate. Therefore we end up with 18 magnitudes and 14 phases to be determined by the fit.

VI. RESULTS

The maximum likelihood fit results in a $B^0 \rightarrow K^+\pi^-\pi^0$ event yield of $N_{sig} = 4583 \pm 122$ events, where the uncertainty is statistical only. When the fit is repeated starting from input parameter values randomly chosen within wide ranges of one order of magnitude above and below the nominal values for the amplitudes and within the $[-\pi, \pi]$ interval for the phases, we observe convergence toward four solutions with minimum values of the negative loglikelihood function (NLL). The best solution is separated by 3.9 units of NLL from the next best solution. The event yield we quote is for the best solution; the spread of signal yields between the four solutions is less than 5 events. The fitted phases Φ , $\bar{\Phi}$ and the CP -asymmetries A_{CP} are given for the best solution in Table IV.

TABLE IV: Results of the best solution. The fractions are the CP -averaged isobar fractions (FF_k) defined with the CP -asymmetries A_{CP} in Section II [Eq. (5)]. The phases Φ for the B^0 decays and $\bar{\Phi}$ for the \bar{B}^0 decays are measured relative to $B^0(\bar{B}^0) \rightarrow \rho^\mp K^\pm$. The first error is statistical and the second is systematic.

	Isobar Fraction (%)	Φ	Φ	A_{CP}
$\rho^-(770)K^+$	$13.60 \pm 1.24 \pm 0.60$	0.00 (fixed)	0.00 (fixed)	$0.14 \pm 0.06 \pm 0.01$
$\rho^-(1450)K^+$	$4.66 \pm 1.42 \pm 0.68$	$1.63 \pm 0.26 \pm 0.12$	$1.63 \pm 0.26 \pm 0.12$	$0.14 \pm 0.06 \pm 0.01$
$\rho^-(1700)K^+$	$1.16 \pm 0.69 \pm 0.26$	$0.52 \pm 0.40 \pm 0.15$	$0.52 \pm 0.40 \pm 0.15$	$0.14 \pm 0.06 \pm 0.01$
$K^{*+}(892)\pi^-$	$5.52 \pm 0.59 \pm 0.18$	$0.74 \pm 0.36 \pm 0.14$	$0.37 \pm 0.36 \pm 0.31$	$-0.30 \pm 0.11 \pm 0.03$
$K^{*0}(892)\pi^0$	$4.53 \pm 0.57 \pm 0.26$	$0.65 \pm 0.29 \pm 0.10$	$-0.00 \pm 0.33 \pm 0.10$	$-0.15 \pm 0.12 \pm 0.02$
$(K\pi)_0^{*+}\pi^-$	$23.60 \pm 1.18 \pm 1.70$	$-2.76 \pm 0.25 \pm 0.08$	$-2.60 \pm 0.30 \pm 0.22$	$0.07 \pm 0.05 \pm 0.01$
$(K\pi)_0^{*0}\pi^0$	$11.90 \pm 1.11 \pm 1.46$	$0.37 \pm 0.26 \pm 0.38$	$-0.11 \pm 0.27 \pm 0.24$	$-0.16 \pm 0.09 \pm 0.04$
N.R.	$5.90 \pm 0.93 \pm 0.80$	$1.00 \pm 0.24 \pm 0.17$	$1.15 \pm 0.27 \pm 0.18$	$0.07 \pm 0.15 \pm 0.04$
$\bar{D}^0\pi^0$	$20.90 \pm 0.85 \pm 2.66$			
D^-K^+	$0.93 \pm 0.23 \pm 0.02$			

The Dalitz plot mass distributions in an enlargement of the low-mass resonance region (masses below 2.0 GeV/ c^2) are shown in Fig. 3. The ρ^- , K^{*+} , and K^{*0} are clearly visible in the $m_{\pi^-\pi^0}$, $m_{K^+\pi^0}$, $m_{K^+\pi^-}$ distributions respectively. We calculate a χ^2 of 772 for 644 bins on the Dalitz plot where at least 25 events are guaranteed to exist in each bin. The distributions of the discriminating variables (m_{ES} , $\Delta E'$ and NN) are shown in Fig. 4. Fitted parameters are given for the four solutions in Table V. We observe that the fit fractions and the CP asymmetries are consistent within less than three standard deviations among the solutions, though the phases differ substantially.

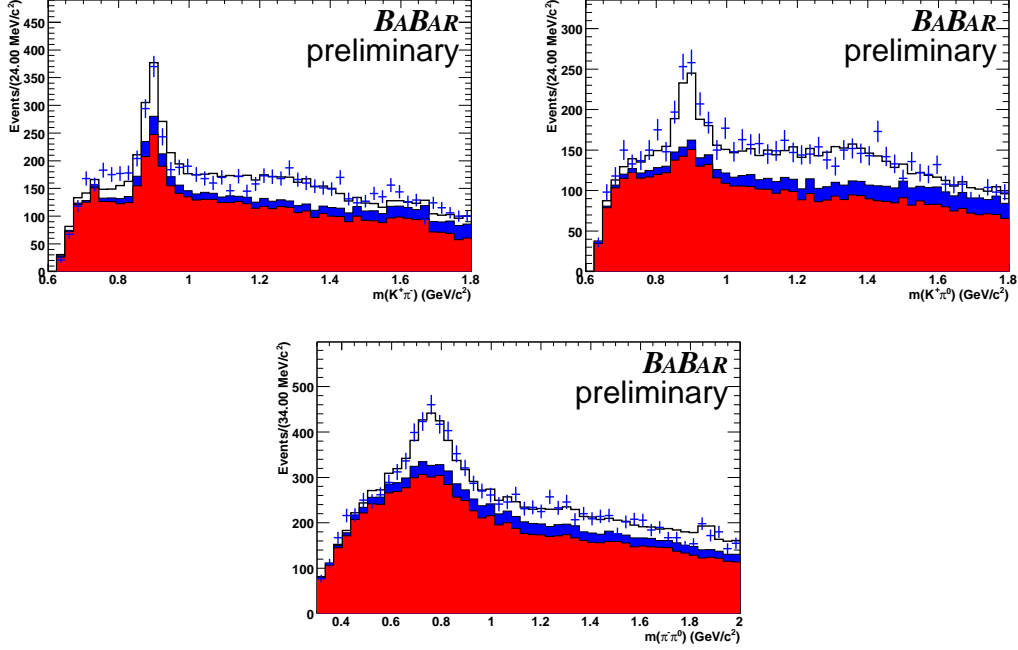


FIG. 3: Mass distributions for: $m_{K^+\pi^-}$ (a), $m_{K^+\pi^0}$ (b) and $m_{\pi^-\pi^0}$ (c). The data are shown as points with error bars. The solid histograms show the projection of the fit result. The blue (dark) and red (gray) shaded areas represent the B background and continuum, respectively.

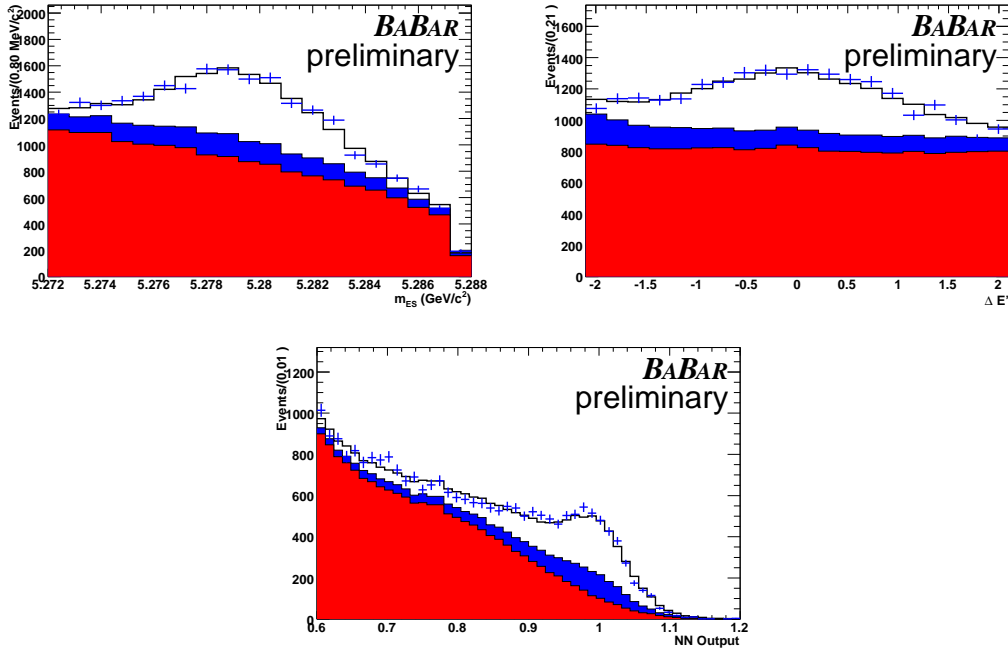


FIG. 4: (a) m_{ES} , (b) $\Delta E'$ and (c) NN distributions. The data are shown as points with error bars. The solid histograms show the projection of the fit result. The blue (dark) and red (gray) shaded areas represent the B background and continuum, respectively.

TABLE V: Results of the four solutions of the fit. The fractions are the CP -averaged isobar fractions (FF_k) defined with the CP -asymmetries A_{CP} in Section II [Eq. (5)]. The phases Φ for the B^0 decays and $\overline{\Phi}$ for the \overline{B}^0 decays are measured relative to $B^0(\overline{B}^0) \rightarrow \rho^\mp \pi^\pm$. The uncertainties are statistical only.

Resonance	Parameter	Solution-I	Solution-II	Solution-III	Solution-IV
	$\Delta(NLL)$	0.00	3.94	7.77	10.57
$\rho^-(770)K^+$	FF (%)	13.60 ± 1.24	13.70 ± 1.25	13.20 ± 1.09	13.40 ± 1.27
	A_{CP}	0.14 ± 0.06	0.17 ± 0.06	0.11 ± 0.06	0.14 ± 0.06
	$\overline{\Phi}$	0 (fixed)	0 (fixed)	0 (fixed)	0 (fixed)
	Φ	0 (fixed)	0 (fixed)	0 (fixed)	0 (fixed)
$\rho^-(1450)K^+$	FF (%)	4.66 ± 1.42	4.13 ± 1.42	4.61 ± 1.56	4.16 ± 1.61
	A_{CP}	0.14 ± 0.06	0.17 ± 0.06	0.11 ± 0.06	0.14 ± 0.06
	$\overline{\Phi}$	1.63 ± 0.26	1.41 ± 0.25	1.64 ± 0.28	1.39 ± 0.27
	Φ	1.63 ± 0.26	1.41 ± 0.25	1.64 ± 0.28	1.39 ± 0.27
$\rho^-(1700)K^+$	FF (%)	1.16 ± 0.69	0.61 ± 0.52	0.78 ± 0.64	0.30 ± 0.43
	A_{CP}	0.14 ± 0.06	0.17 ± 0.06	0.11 ± 0.06	0.14 ± 0.06
	$\overline{\Phi}$	0.52 ± 0.40	0.42 ± 0.51	0.38 ± 0.53	0.07 ± 0.78
	Φ	0.52 ± 0.40	0.42 ± 0.51	0.38 ± 0.53	0.07 ± 0.78
$K^{*+}(892)\pi^-$	FF (%)	5.52 ± 0.59	5.54 ± 0.61	5.92 ± 1.21	5.88 ± 0.63
	A_{CP}	-0.30 ± 0.11	-0.30 ± 0.11	-0.21 ± 0.11	-0.22 ± 0.11
	$\overline{\Phi}$	0.74 ± 0.36	0.66 ± 0.36	-3.10 ± 0.37	3.09 ± 0.36
	Φ	0.37 ± 0.36	2.58 ± 0.36	0.36 ± 0.36	2.61 ± 0.35
$K^{*0}(892)\pi^0$	FF (%)	4.53 ± 0.57	4.61 ± 0.57	4.63 ± 0.59	4.69 ± 0.58
	A_{CP}	-0.15 ± 0.12	-0.16 ± 0.12	-0.15 ± 0.12	-0.15 ± 0.12
	$\overline{\Phi}$	0.65 ± 0.29	0.58 ± 0.30	0.34 ± 0.30	0.25 ± 0.30
	Φ	-0.00 ± 0.33	0.24 ± 0.35	-0.03 ± 0.34	0.19 ± 0.35
$(K\pi)_0^{*+}\pi^-$	FF (%)	23.60 ± 1.18	24.90 ± 1.17	24.90 ± 1.19	26.10 ± 1.16
	A_{CP}	0.07 ± 0.05	0.02 ± 0.05	0.11 ± 0.05	0.06 ± 0.05
	$\overline{\Phi}$	-2.76 ± 0.25	-2.84 ± 0.26	-0.50 ± 0.32	-0.57 ± 0.31
	Φ	-2.60 ± 0.30	-0.50 ± 0.31	-2.60 ± 0.31	-0.45 ± 0.31
$(K\pi)_0^{*0}\pi^0$	FF (%)	11.90 ± 1.11	17.80 ± 1.24	16.60 ± 1.09	22.80 ± 1.17
	A_{CP}	-0.16 ± 0.09	-0.43 ± 0.08	0.17 ± 0.07	-0.14 ± 0.06
	$\overline{\Phi}$	0.37 ± 0.26	0.29 ± 0.27	0.20 ± 0.22	0.11 ± 0.22
	Φ	-0.11 ± 0.27	0.26 ± 0.23	-0.12 ± 0.28	0.26 ± 0.23
NR	FF (%)	5.90 ± 0.93	3.98 ± 0.81	5.40 ± 1.02	3.49 ± 1.09
	A_{CP}	0.07 ± 0.15	0.64 ± 0.21	-0.04 ± 0.19	0.54 ± 0.22
	$\overline{\Phi}$	1.00 ± 0.24	0.91 ± 0.24	-0.93 ± 0.26	-1.04 ± 0.26
	Φ	1.15 ± 0.27	-1.22 ± 0.34	1.16 ± 0.29	-1.21 ± 0.34
$\overline{D}^0\pi^0$	FF (%)	20.90 ± 0.85	20.80 ± 0.85	20.70 ± 0.93	20.60 ± 0.86
D^-K^+	FF (%)	0.93 ± 0.23	0.96 ± 0.23	0.98 ± 0.23	1.02 ± 0.24

VII. SYSTEMATIC UNCERTAINTIES

Variations around the nominal fit are tried to study the dominant systematic effects, summarized in Table VI. For each parameter of interest (FF , A_{CP} , Φ), the positive (negative) deviations from each effect are summed in quadrature to obtain total upward (downward) systematic errors δ_+ (δ_-). Systematic effects are studied by varying the number of resonances contributing to the signal model, the lineshape parameters of the resonances in the signal model, the yields of the nominally fixed B-backgrounds, and the shape of the continuum Dalitz PDF. The intrinsic bias of the fit as measured in MC studies, is also included as a source of systematic error.

- To estimate the contribution of other resonances, we fit the on resonance data with extended signal models including one *extra*-resonance in addition to those in the nominal signal model. The $K_2^{*0}(1430)\pi^0$, $K_2^{*+}(1430)\pi^-$, $K^{*0}(1680)\pi^0$ and $K^{*+}(1680)\pi^-$ have been added to the nominal model, and fits with these resonances show some improvement in likelihood. In the best solutions obtained with these extended models the addition resonances did not significantly interfere with those in the nominal model. The variations of the physical parameters due to additional resonances are recorded as *Dalitz Plot Model* uncertainties in Table VI.
- The variations of the physical parameters of the resonances in the nominal signal model are recorded as *Lineshape* systematic uncertainties.
- Variations of the PDF shape parameters are recorded as *PDF Shape Parameter* systematic uncertainties. Specifically, mismodeling of the continuum square Dalitz plot PDF (Section V.B) is studied by recreating the PDF with numerous smoothing parameters and varying the amount of B-background subtracted from the m_{ES} sideband by 50%. A small difference in the shape of the TM-signal NN distribution between data and MC is also studied.
- To estimate the *Fit Bias* uncertainties inherent in our fit technique, we record the fitted biases and spreads in fits performed on large Monte Carlo samples with both signal and background events generated with their nominal PDFs.
- Each of the nominally fixed B-background yields is allowed to vary freely in a series of fits to data. The variations of B-background yields are recorded as *B-background* systematic uncertainties.

VIII. SUMMARY

We have performed an amplitude analysis of the $B^0 \rightarrow K^+\pi^-\pi^0$ decay. We have measured the CP -averaged fit fractions, CP -asymmetries and phases of the decay precesses to the intermediate states with $\rho^-(770)K^+$, $\rho^-(1450)K^+$, $\rho^-(1700)K^+$, $K^*(892)^{+,0}\pi^{-,0}$, $(K\pi)_0^{*,+0}\pi^{-,0}$. We find a satisfactory solution that provides a significant constraint on the phases of the resonances. For this solution, the CP asymmetries are consistent with zero in all quasi two-body channels. Three further solutions were found, though all had an NLL worse by 3.9 units, or more. Additionally, we measure the CP -averaged fit fractions for the decays $B^0 \rightarrow \bar{D}^0\pi^0 \rightarrow K^+\pi^-\pi^0$ and $B^0 \rightarrow D^-K^+ \rightarrow K^+\pi^-\pi^0$.

TABLE VI: Summary of systematic uncertainties.

Resonance		Fit Fraction (%)	A_{cp}	Φ	Φ
$\rho^-(770)K^+$	Dalitz Plot Model	0.500	0.003	Fixed	Fixed
	PDF Shape Parameters	0.224	0.005	Fixed	Fixed
	B Backgrounds	0.071	0.001	Fixed	Fixed
	Lineshapes	0.229	0.003	Fixed	Fixed
	Fit Bias	0.015	0.004	Fixed	Fixed
	Total	0.598	0.008	Fixed	Fixed
$\rho^-(1450)K^+$	Dalitz Plot Model	0.560	-	0.060	0.060
	PDF Shape Parameters	0.255	-	0.039	0.039
	B Backgrounds	0.038	-	0.014	0.014
	Lineshapes	0.232	-	0.088	0.088
	Fit Bias	0.170	-	0.022	0.022
	Total	0.680	-	0.116	0.116
$\rho^-(1700)K^+$	Dalitz Plot Model	0.070	-	0.077	0.077
	PDF Shape Parameters	0.042	-	0.038	0.038
	B Backgrounds	0.009	-	0.009	0.009
	Lineshapes	0.216	-	0.120	0.120
	Fit Bias	0.110	-	0.037	0.037
	Total	0.256	-	0.152	0.152
$K^{*+}(892)\pi^-$	Dalitz Plot Model	0.070	0.020	0.112	0.260
	PDF Shape Parameters	0.154	0.026	0.021	0.080
	B Background	0.025	0.004	0.013	0.009
	Lineshapes	0.030	0.006	0.061	0.147
	Fit Bias	0.020	0.004	0.047	0.038
	Total	0.175	0.034	0.138	0.312
$K^{*0}(892)\pi^0$	Dalitz Plot Model	0.200	0.010	0.065	0.065
	PDF Shape Parameters	0.128	0.005	0.020	0.031
	B Background	0.028	0.002	0.015	0.012
	Lineshapes	0.039	0.004	0.048	0.065
	Fit Bias	0.087	0.005	0.046	0.012
	Total	0.257	0.022	0.096	0.098
$(K\pi)_0^{*+}$	Dalitz Plot Model	1.200	0.009	0.050	0.190
	PDF Shape Parameters	1.166	0.007	0.022	0.079
	B Background	0.071	0.001	0.012	0.015
	Lineshapes	0.166	0.004	0.047	0.121
	Fit Bias	0.260	0.006	0.041	0.030
	Total	1.703	0.014	0.084	0.218
$(K\pi)_0^{*0}$	Dalitz Plot Model	1.400	0.033	0.370	0.225
	PDF Shape Parameters	0.173	0.016	0.056	0.032
	B Background	0.071	0.005	0.025	0.016
	Lineshapes	0.224	0.017	0.071	0.071
	Fit Bias	0.300	0.003	0.044	0.009
	Total	1.461	0.041	0.384	0.239
NR	Dalitz Plot Model	0.240	0.017	0.119	0.110
	PDF Shape Parameters	0.744	0.035	0.106	0.060
	B Background	0.042	0.003	0.014	0.014
	Lineshapes	0.134	0.019	0.067	0.117
	Fit Bias	0.120	0.003	0.009	0.034
	Total	0.803	0.044	0.174	0.175
$\overline{D}^0\pi^0$	Dalitz Plot Model	0.500	-	-	-
	PDF Shape Parameters	2.606	-	-	-
	B Background	0.150	-	-	-
	Lineshapes	0.071	-	-	-
	Fit Bias	0.073	-	-	-
	Total	2.660	-	-	-
D^-K^+	Dalitz Plot Model	0.010	-	-	-
	PDF Shape Parameters	0.015	-	-	-
	B Background	0.002	-	-	-
	Lineshapes	0.013	-	-	-
	Fit Bias	0.001	-	-	-
	Total	0.022	-	-	-

IX. ACKNOWLEDGMENTS

We are grateful for the extraordinary contributions of our PEP-II colleagues in achieving the excellent luminosity and machine conditions that have made this work possible. The success of this project also relies critically on the expertise and dedication of the computing organizations that support *BABAR*. The collaborating institutions wish to thank SLAC for its support and the kind hospitality extended to them. This work is supported by the US Department of Energy and National Science Foundation, the Natural Sciences and Engineering Research Council (Canada), the Commissariat à l’Energie Atomique and Institut National de Physique Nucléaire et de Physique des Particules (France), the Bundesministerium für Bildung und Forschung and Deutsche Forschungsgemeinschaft (Germany), the Istituto Nazionale di Fisica Nucleare (Italy), the Foundation for Fundamental Research on Matter (The Netherlands), the Research Council of Norway, the Ministry of Education and Science of the Russian Federation, Ministerio de Educación y Ciencia (Spain), and the Science and Technology Facilities Council (United Kingdom). Individuals have received support from the Marie-Curie IEF program (European Union) and the A. P. Sloan Foundation.

-
- [1] N. Cabibbo, Phys. Rev. Lett. **10**, 531 (1963); M. Kobayashi and T. Maskawa, Prog. Theor. Phys. **49**, 652 (1973).
 - [2] H.R. Quinn and A.E. Snyder, Phys. Rev. D **48**, 2139 (1993).
 - [3] *BABAR* Collaboration, B. Aubert *et al.*, Phys. Rev. D **76**, 012004 (2007).
 - [4] Belle Collaboration, A. Kusaka *et al.*, Phys. Rev. Lett. **98**, 221602 (2007).
 - [5] M. Ciuchini, M. Pierini and L. Silvestrini, Phys. Rev. D **74**, 051301 (2006).
 - [6] M. Gronau, D. Pirjol, A. Soni and J. Zupan, Phys. Rev. D **75**, 014002 (2007).
 - [7] Throughout the paper, whenever a mode is given, the charge conjugate is also implied.
 - [8] *BABAR* Collaboration, submitted to PRD, [{arXiv:hep-ex/0711.4417}](#).
 - [9] CLEO Collaboration, E. Eckhart *et al.*, Phys. Rev. Lett. **89**, 251801 (2002).
 - [10] Belle Collaboration, P. Chang *et al.*, Phys. Lett. B **599**, 148 (2004).
 - [11] CLEO Collaboration, C. P. Jessop *et al.*, Phys. Rev. Lett. **85**, 2881 (2000).
 - [12] *BABAR* Collaboration, B. Aubert *et al.*, Phys. Rev. D **76**, 011103 (2007).
 - [13] *BABAR* Collaboration, B. Aubert *et al.*, Phys. Rev. D **72**, 072003 (2005); Erratum-ibid. Phys. Rev. D **74**, 099903 (2006).
 - [14] Belle Collaboration, A. Garmash *et al.*, Phys. Rev. Lett. **96**, 251803 (2006).
 - [15] *BABAR* Collaboration, B. Aubert *et al.*, Phys. Rev. D **73**, 031101 (2006).
 - [16] Belle Collaboration, A. Garmash *et al.*, Phys. Rev. D **75**, 012006 (2007).
 - [17] H. Y. Cheng, C. K. Chua and A. Soni, Phys. Rev. D **76**, 094006 (2007).
 - [18] J. Blatt and V. Weisskopf, “*Theoretical Nuclear Physics*”, John Wiley & Sons, New York, 1956.
 - [19] D. Asner, [{arXiv:hep-ex/0410014}](#).
 - [20] C. Zemach, Phys. Rev. **133**, B1201 (1964).
 - [21] D. Aston *et al.*, Nucl. Phys. B **296**, 493 (1988).
 - [22] Particle Data Group, W.-M. Yao *et al.*, Journal of Physics G **33**, 1 (2006).
 - [23] G.J. Gounaris and J.J. Sakurai, Phys. Rev. Lett. **21**, 244 (1968).
 - [24] CMD-2 Collaboration, R.R. Akhmetshin *et al.*, Phys. Lett. B **257**, 161 (2002).
 - [25] DM2 Collaboration, D. Bisello *et al.*, Phys. Lett. B **220**, 321 (1989).
 - [26] P. Estabrooks, Phys. Rev. D **19**, 2678 (1979).
 - [27] *BABAR* Collaboration, B. Aubert *et al.*, Nucl. Instrum. Methods Phys. Res., Sect. A **479**, 1 (2002).
 - [28] GEANT4 Collaboration, S. Agostinelli *et al.*, Nucl. Instrum. Methods Phys. Res., Sect. A **506**, 250 (2003).
 - [29] P. Gay, B. Michel, J. Proriol and O. Deschamps, “*Tagging Higgs Bosons in Hadronic LEP-2 Events with Neural Networks*”, in Pisa 1995, New computing techniques in physics research, 725 (1995).
 - [30] *BABAR* Collaboration, B. Aubert *et al.*, Phys. Rev. Lett. **94**, 161803 (2005).
 - [31] K. S. Cranmer, Comput. Phys. Commun. **136**, 198 (2001).
 - [32] ARGUS Collaboration, (H. Albrecht *et al.*), Z. Phys. C **48**, 543 (1990).
 - [33] Heavy Flavor Averaging Group (HFAG), E. Barberio *et al.*, [{arXiv:hep-ex/0704.3575}](#).